Surface Polyethylene Glycol Conformation Influences the Protein Corona of Polyethylene Glycol-Modified Single-Walled Carbon Nanotubes: Potential Implications on Biological Performance

Cristiano Sacchetti,[†,∥] Khatereh Motamedchaboki,[†] Andrea Magrini,[‡] Graziana Palmieri,[§] Maurizio Mattei,[§] Sergio Bernardini,[§] Nicola Rosato,[⊥] Nunzio Bottini,[∥] and Massimo Bottini[†,⊥,*]

[†]Sanford-Burnham Medical Research Institute, 10901 North Torrey Pines Road, La Jolla, California 92037, United States, [‡]Department of Biomedicine and Prevention, [§]Department of Biology, and [⊥]Department of Experimental Medicine and Surgery, University of Rome Tor Vergata, Via Montpellier 1, 00133 Rome, Italy, and [∥]Division of Cellular Biology, La Jolla Institute for Allergy and Immunology, 9420 Athena Circle, La Jolla, California 92037, United States

ABSTRACT Investigation of the nanoparticle protein corona, the shell of plasma proteins formed around nanoparticles immediately after they enter the bloodstream, is a benchmark in the study of the applications of nanoparticles in all fields of medicine, from pharmacology to toxicology. We report the first investigation of the protein corona adsorbed onto single-walled carbon nanotubes modified with 2 kDa molecular weight polyethylene glycol chains [PEG(2k)-modified SWCNTs or PEG2-SWCNTs] by using a large-scale gel-based proteomics method on biological replicates. More than 240 plasma proteins were selected, and their differences were analyzed among PEG2-SWCNTs differing in surface charge and PEG conformation. The protein corona of PEG2-SWCNTs showed that coagulation proteins, immunoglobulins, apolipoproteins, and proteins of the complement system were among the proteins bound by PEG2-SWCNTs and that their recruitment was independent from the isoelectric point, molecular weight, total hydrophobicity, and number of polyaromatic residues of the proteins. Statistical analysis on protein relative abundance revealed that PEG conformation had a higher influence on the PEG2-SWCNTs' protein corona repertoire than nanotube surface charge. PEG conformation also affected the biological performance of PEG2-SWCNTs. A change in PEG conformation from mushroom to mushroom-brush transition affected the competitive adsorption of the major constituents of the protein corona of PEG2-SWCNTs and promoted shorter blood circulation time, faster renal excretion, and higher relative spleen *versus* liver uptake of PEG2-SWCNTs. Our data suggest that the protein corona, along with steric stabilization, may mediate the action of PEG conformation on the pharmacokinetic profile of PEG-modified SWCNTs.

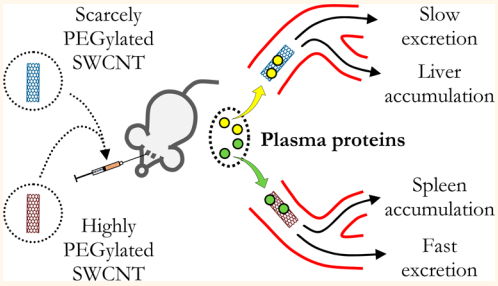

KEYWORDS: carbon nanotubes · polyethylene glycol · protein corona · mass spectrometry · pharmacokinetic profile · steric stabilization

With the advent of nanotechnology in the past decade, several new types of nanoscopic particles (nanoparticles) are under development for innovative biomedical applications, including drug delivery, *in vivo* imaging, tissue regeneration, and ablation of tumors.[1] The translation potential of these new materials is currently limited by their bioavailability and biocompatibility, which are often unknown or suboptimal. Poly(ethylene glycol) (PEG), as well as other types of repelling hydrophilic polymers, has been widely used as a surface modification agent to ameliorate the biological performance of nanoparticles (organ accumulation, biocompatibility, toxicity, *etc.*). However, a clear picture of the mechanisms underlying the effects of PEG modification on the nanoparticle pharmacokinetic profile is still missing. PEG has been traditionally thought to decrease nanoparticle recognition (and uptake) by phagocytic

* Address correspondence to mbottini@sanfordburnham.org.

Received for review August 14, 2012 and accepted February 17, 2013.

Published online February 18, 2013
10.1021/nn400409h

cells of the reticulo endothelial system (RES) by forming a surface-random cloud that abrogates the formation of the protein corona—the shell of plasma proteins formed around nanoparticles immediately after they enter the bloodstream—and sterically stabilizes the nanoparticles against aggregation and receptor-mediated recognition.[2−7] Nevertheless, several studies have shown that PEG modification does not abrogate adsorption of plasma proteins onto spherical nanoparticles.[8−10] Furthermore, investigations into the role of the protein corona on nanoparticle biological performance show contradictory results. For instance, Dos Santos *et al.* hypothesized that the presence of the protein corona does not correlate with differences in the pharmacokinetic profile of PEG-modified liposomes,[8] whereas Chonn *et al.* and Schreier *et al.* have highlighted the involvement of plasma proteins in liposomal biodistribution.[11,12] A better knowledge of the protein corona and the relationship between its repertoire, nanoparticle physicochemical properties, and nanoparticle behavior at both the organism and cellular level is a key step in the development of safe and efficient nanotechnology-based drugs.[13]

Among the recent nanotechnology-derived particles, PEG-modified single-walled carbon nanotubes (PEG-modified SWCNTs or PEG-SWCNTs) are receiving increased attention for biomedical applications because of their excellent intrinsic properties and biological performance.[14] PEG-SWCNTs were able to spontaneously enter several cell types,[15−17] displayed relatively long blood circulation time,[18−20] and as of yet their administration into mice did not elicit serious immune and/or inflammatory responses.[21] The biological performance of PEG-SWCNTs at the animal level has been reported to depend on their level of aggregation[22,23] and the nature and length of PEG chains.[24] However, a clear structure−function relationship did not emerge from these studies, and other molecular determinants of PEG-SWCNT biological behavior after injection into the bloodstream, including the effects of the protein corona, have not been taken in account yet. Herein, we gathered information about the protein corona bound by SWCNTs modified with 2 kDa molecular weight PEG chains [PEG(2k)-modified SWCNTs or PEG2-SWCNTs] differing in surface charge and PEG conformation by a gel-based proteomics approach using protein identification from 1D SDS-PAGE gels followed by long one-dimensional liquid chromatography coupled mass spectrometry analysis. The data about protein relative abundance for the PEG2-SWCNTs' protein coronas were statistically analyzed in biological replicates to correlate the adsorption of plasma proteins to specific properties of PEG2-SWCNTs while avoiding artifacts caused by proteome variability. We found that the PEG modification did not abrogate the absorption of plasma proteins onto SWCNTs and that the PEG conformation influences the pattern of adsorbed proteins more than charge does. We also investigated the effects of PEG conformation on the biodistribution of PEG2-SWCNTs. A change in PEG conformation from mushroom to mushroom-brush transition configuration promoted shorter blood circulation time, faster renal excretion, and higher relative spleen *versus* liver uptake of PEG2-SWCNTs. Here we discuss potential implications of the corona repertoire on the pharmacokinetic behavior of PEG2-SWCNTs. We found that a transient depletion of one of the constituent of the PEG2-SWCNTs' protein corona [β-2-glycoprotein (ApoH)] from the mouse bloodstream affected the relative spleen *versus* liver uptake of PEG2-SWCNTs. Our data suggest that the protein corona, along with steric stabilization and nanotube properties, may mediate the action of PEG conformation on the pharmacokinetic profile of PEG2-SWCNTs.

RESULTS

Fabrication and Characterization of PEG2-SWCNTs. PEG2-SWCNTs were fabricated through noncovalent [PEG(2k)-coated SWCNTs or cPEG2-SWCNTs] and covalent [PEG(2k)-functionalized SWCNTs or fPEG2-SWCNTs] chemical protocols. cPEG2-SWCNTs were fabricated by adsorption of phospholipids modified with linear 2 kDa amino-terminated PEG chains onto pristine SWCNTs (cPEG2-SWCNT-a) and subsequent capping of the terminal amino groups with either methyl groups (cPEG2-SWCNT-m) or near-infrared (NIR)-emitting fluorochromes (cPEG2-SWCNT-750) (Figure 1A). fPEG2-SWCNTs were fabricated by amidation of oxidized SWCNTs with linear 2 kDa amino-PEG-Boc chains, followed by Boc deprotection (fPEG2-SWCNT-a) and capping of the terminal amino groups with either methyl groups (fPEG2-SWCNT-m) or NIR-emitting fluorochromes (fPEG2-SWCNT-750) (Figure 1D).

PEG2-SWCNTs were characterized by atomic force microscope (AFM), elemental analysis, and dynamic light scattering. The physical properties are listed in Table 1. PEG2-SWCNTs were free from metallic impurities, sterile, and stably dispersed in high saline solutions for months at room temperature without showing any sign of precipitation (data not shown). cPEG2-SWCNTs and fPEG2-SWCNTs had a PEG density of ~0.1 and ~0.4 mmol per gram of nanotube material, respectively. AFM images showed that both types of PEG2-SWCNTs were formed by individual/very scarcely aggregated particles and had similar length distributions centered at ~100 nm (Figure 1B,E). AFM imaging was also used to investigate the morphology of PEG2-SWCNTs. cPEG2-SWCNTs had a needle-like shape and displayed AFM longitudinal cross sections that were not uniform and with maximum heights of a few nanometers (Figure 1C). More than 50% of the imaged cPEG2-SWCNTs showed longitudinal cross sections displaying flat ~1 nm tall portions extending for several tens of nanometers (black arrows in Figure 1C).

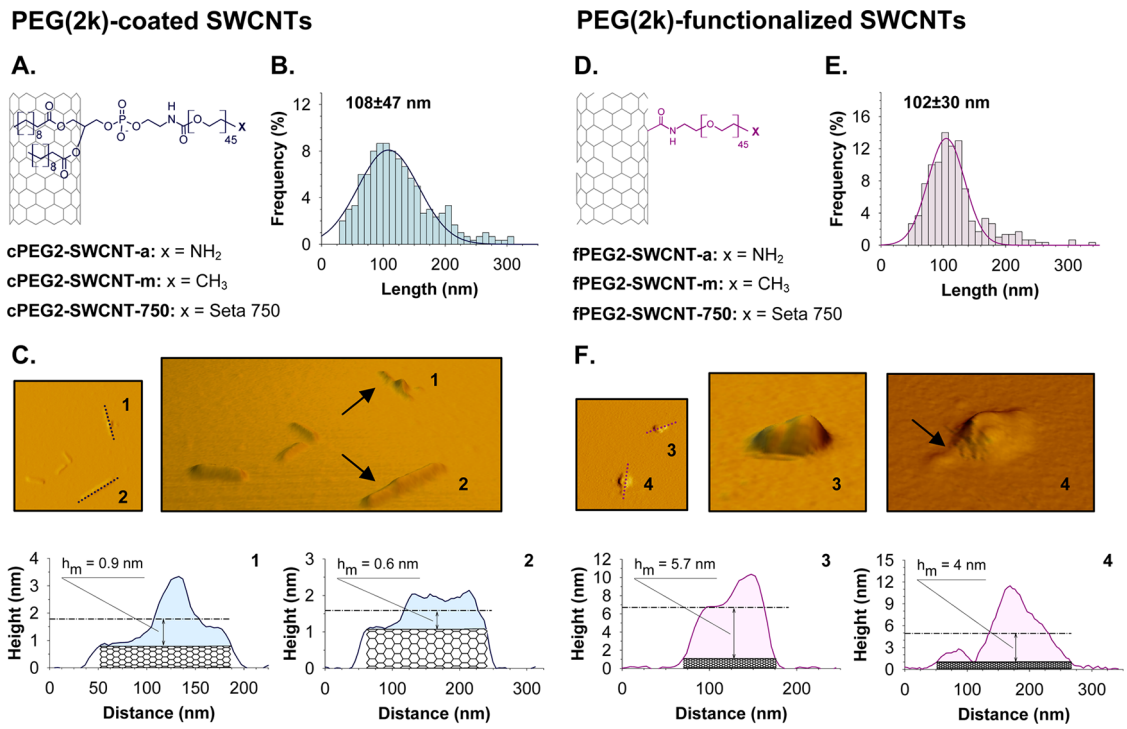

Figure 1. PEG2-SWCNTs used for studying interactions with human plasma proteins and biological performance. (A,D) PEG(2k)-coated SWCNTs (cPEG2-SWCNTs) were obtained by adsorption of PEG-modified phospholipids onto the sidewalls of pristine SWCNT sidewalls (A), whereas PEG(2k)-functionalized SWCNTs (fPEG2-SWCNTs) were obtained by amidation of carboxylic acid groups introduced on nanotube sidewalls and open ends by strong acid treatment (D). We investigated the protein corona and biological performance of PEG2-SWCNTs carrying linear 2 kDa molecular weight PEG chains having amino groups, methyl groups, or NIR-emitting dyes (Seta750) at their distal ends. (B,E) Length distributions for cPEG2-SWCNT-a (B) and fPEG2-SWCNT-a (E) ($N = 300$). (C,F) AFM (amplitude) images of cPEG2-SWCNTs (C, scan size 600 × 600 nm) and fPEG2-SWCNTs (F, scan size 750 × 750 nm). The three-dimensional reconstruction, longitudinal cross sections, and values for the average height of PEG coverage (h_m) for representative cPEG2-SWCNT-a and fPEG2-SWCNT-a (numbered PEG2-SWCNTs in the AFM images) are reported. The black arrows indicate the portions of unmodified SWCNT sidewall that was exposed because it was devoid of PEG coverage.

TABLE 1. Properties of PEG2-SWCNTs Used for Studying Interactions with Human Plasma Proteins[a]

	1	2	3	4	5
surface chemical group	$-NH_2$	$-CH_3$	−Seta750	$-CH_3$	−Seta750
surface charge in H_2O (mV)	2	−39.4	−52.3	−41.7	−53.9
surface charge in PBS (mV)	5.3	−2.2	−11	−2	−8
length (nm)		108 ± 47^b		102 ± 30^b	
PEG density (mmol g^{-1})		0.12 ± 0.04^c		0.39 ± 0.1^c	
h_m (nm)		0.9 ± 0.6^b		7.1 ± 2.8^b	

[a] PEG2-SWCNTs were characterized by dynamic light scattering (surface charge) and atomic force microscope [length and PEG average height (h_m)]. Values of h_m were calculated as the ratio between the net PEG area upon a SWCNT and the length of the SWCNT. PEG density (mmol per gram of nanotube material) was calculated by both measuring the amino groups on cPEG2-SWCNT-a and fPEG2-SWCNT-a (Kaiser Test) and measuring the fluorochromes on cPEG2-SWCNT-750 and fPEG2-SWCNT-750.[17] For brevity: **1** = cPEG2-SWCNT-a; **2** = cPEG2-SWCNT-m; **3** = cPEG2-SWCNT-750; **4** = fPEG2-SWCNT-m; **5** = fPEG2-SWCNT-750. [b] Values of length and h_m were similar among cPEG2-SWCNTs (fPEG2-SWCNTs) because cPEG2-SWCNT-m (fPEG2-SWCNT-m) and cPEG2-SWCNT-750 (fPEG2-SWCNT-750) were fabricated by capping the amino-PEG terminal groups on cPEG2-SWCNT-a (fPEG2-SWCNT-a) with methyl groups and Seta750, respectively. [c] Values of PEG density calculated by Kaiser test. The values of PEG density calculated by measuring the fluorochromes on cPEG2-SWCNT-750 and fPEG2-SWCNT-750 were very close to those calculated by Kaiser test.

fPEG2-SWCNTs had a globular shape, and their longitudinal cross sections showed maximum heights up to more than 10 nm (Figure 1F). Approximately 20% of the nanotubes showed a maximum height of ∼20 nm. Only a low percentage (<10%) of fPEG2-SWCNTs showed flat ∼1 nm tall portions extending just a few nanometers in their longitudinal cross sections (black arrow in Figure 1F). Since we used SWCNTs with a nominal 1.4 nm diameter according to the supplier, the flat ∼1 nm tall portion in longitudinal cross sections of PEG2-SWCNTs was interpreted as the unmodified sidewall of SWCNTs that was exposed because it was devoid of PEG coverage.

In order to qualitatively investigate the conformation of PEG chains decorating the sidewalls of PEG2-SWCNTs, we collected the AFM cross-section curves for 40 PEG2-SWCNTs (20 curves for each type of PEG2-SWCNTs) and calculated their PEG average height (h_m) as the ratio between the net PEG area upon a SWCNT and the length of the SWCNT (the net PEG area—colored areas in Figure 1C,F—was calculated by subtracting the area of the SWCNT from the area under the AFM cross-section curve). We found that h_m was ∼1 and ∼7 nm for cPEG2-SWCNTs and fPEG2-SWCNTs, respectively (Table 1). Moreover, we found that the small fraction of fPEG2-SWCNTs displaying a maximum height of ∼20 nm had an h_m equal to ∼14 nm.

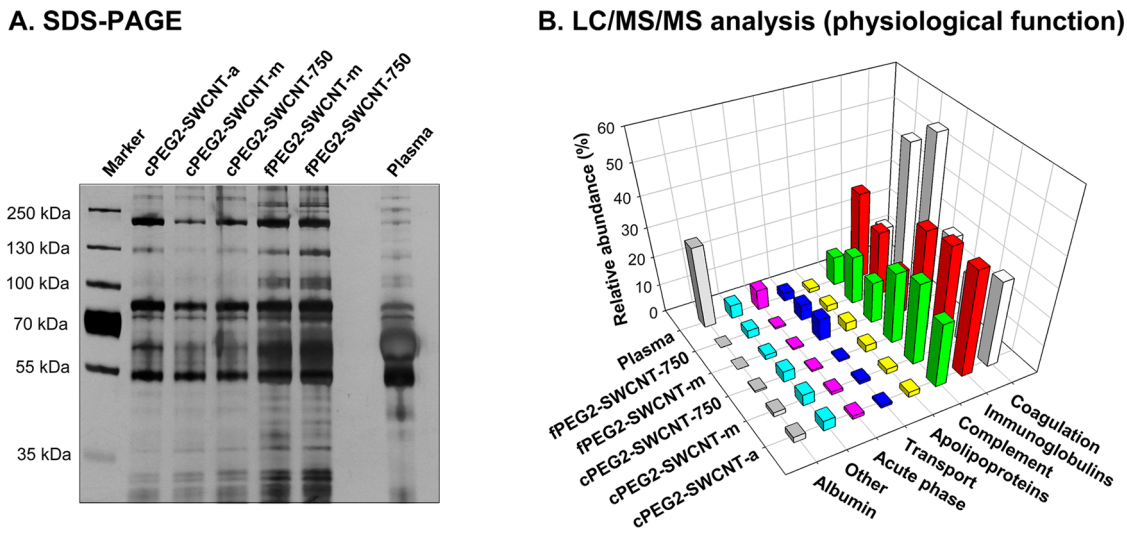

Figure 2. Relative abundance of human plasma proteins adsorbed onto PEG2-SWCNTs. Samples of PEG2-SWCNTs incubated with human plasma proteins at 37 °C and free plasma proteins were separated on 1D SDS-PAGE (A). Tryptic digested proteins were analyzed with a long one-dimensional reversed phase liquid chromatography coupled mass spectrometry. More than 500 proteins were identified. Approximately 240 proteins with nonzero DPSC values for at least one sample among plasma and the five PEG2-SWCNTs were selected and grouped according to their physiological functions. The donor-averaged relative abundances for these groups were calculated for PEG2-SWCNTs and free plasma (B).

Since AFM measurements were recorded in air, we assumed that the PEG chains were collapsed during the measurements because of dehydration and $h_m \sim 14$ nm corresponded to the thickness of the polymeric shell composed by 2 kDa molecular weight PEG chains in brush configuration. This assumption, the AFM longitudinal cross sections, and the calculated values for h_m suggested that cPEG2-SWCNTs displayed PEG chains mostly lying on the nanotubes' sidewall in a mushroom conformation, whereas fPEG2-SWCNTs had PEG chains protruding from the nanotubes' sidewall in a mushroom-brush transition conformation.[25−28]

Human Plasma Protein Corona of PEG2-SWCNTs. Mapping of human plasma proteins associated with PEG2-SWCNTs was studied by a multistep method: incubation of nanoparticles (cPEG2-SWCNT-a, cPEG2-SWCNT-m, cPEG2-SWCNT-750, fPEG2-SWCNT-m, and fPEG2-SWCNT-750) with plasma at 37 °C for 1 h, washing the unbound proteins, protein separation by one-dimensional gel electrophoresis (Figure 2A), identification by a gel-based proteomics approach using protein identification from 1D SDS-PAGE gels by long one-dimensional liquid chromatography coupled mass spectrometry (LC/MS/MS) analysis, and relative protein quantification by protein spectral count.[29−32]

First, we investigated the relative abundance of plasma proteins adsorbed onto PEG2-SWCNTs using data from three biological replicates (independent, healthy donors). More than 500 proteins were identified. Gene ontology (GO) and differential protein spectral count (DPSC) analyses of the identified proteins were carried out using QTools.[33] The GO analysis provided information about the localization (intra- or extracellular), molecular function, and biological processes for each protein indentified by LC/MS/MS analysis. We selected the 240 proteins with nonzero DPSC values for at least one sample among plasma and the five PEG2-SWCNTs, grouped them according to their physiological function, then reported the donor-averaged relative abundance for each functional group of proteins (Figure 2B) and the donor-averaged relative abundance for the proteins in each group (Figure 3: coagulation proteins were divided into two subgroups by function of their abundance in the PEG2-SWCNTs' protein coronas, whereas complement proteins were divided into C1−C9 proteins and factors). These data clearly showed differences in the composition of the PEG2-SWCNTs' coronas driven by nanoparticle properties and protein physiological functions. Coagulation proteins, in particular, fibrinogen (HFG), were the major plasma proteins bound by fPEG2-SWCNTs (Figures 2B and 3A), whereas more than one-third of the cPEG2-SWCNTs' corona was composed by immunoglobulins (Ig) (Figure 3C). α-2-Macroglobulin was the most abundant protein of the cPEG2-SWCNT-a's corona, whereas fibronectin did not bind onto cPEG2-SWCNT-a and cPEG2-SWCNT-m (Figure 3A). The highest fractional binding of complement proteins C1−C9 was found on cPEG2-SWCNTs (Figure 3E), whereas fPEG2-SWCNTs showed the highest fractional binding of acute phase proteins, in particular, inter-α-trypsin inhibitor H4 (ITIH4) (Figure 3H). We also grouped the selected proteins by function of their isolectric point, molecular weight, total hydrophobicity, and total number of polyaromatic residues (Supporting Information Figure S1). However, these data did not show any striking differences among the investigated PEG2-SWCNTs.

Next, we statistically analyzed the differences in relative abundance for plasma proteins among the PEG2-SWCNTs' coronas and plasma using a nonparametric Mann–Whitney U statistic (Table S1). Our analysis showed that

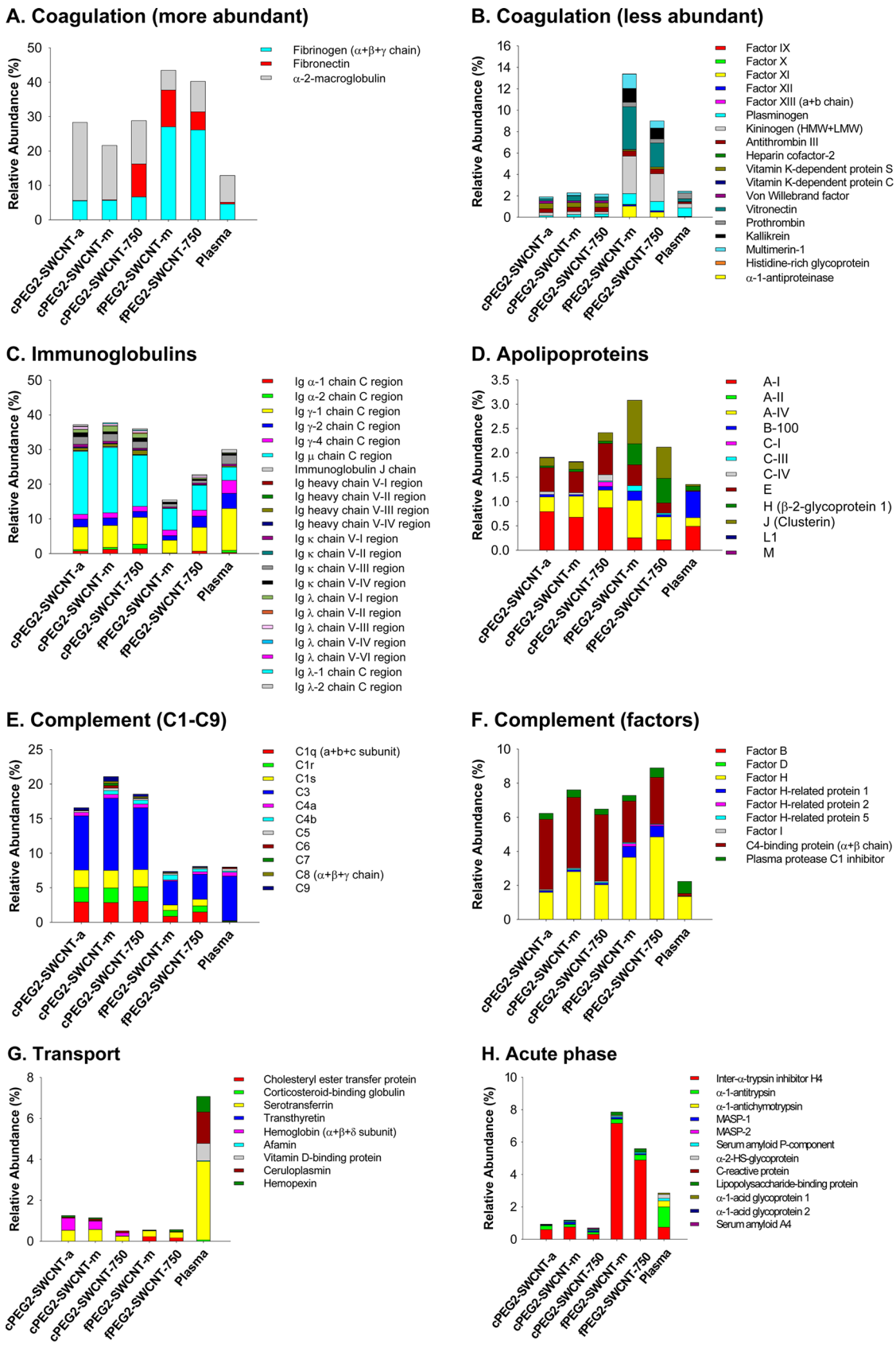

Figure 3. continued

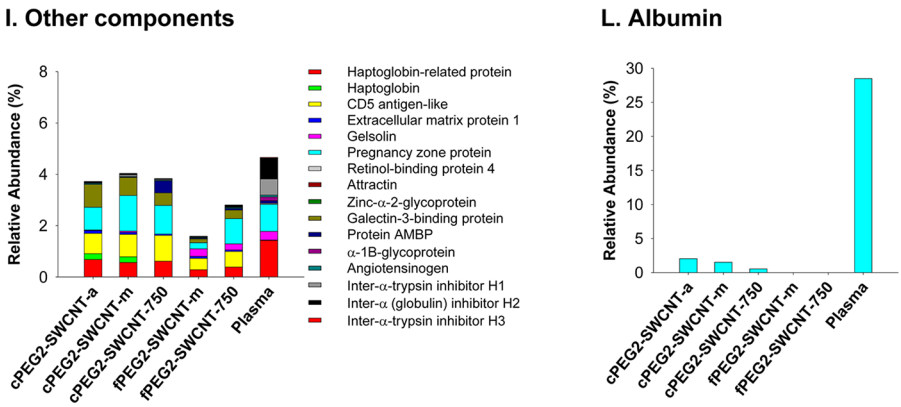

Figure 3. Relative abundance of human plasma proteins adsorbed onto PEG2-SWCNTs. Samples of PEG2-SWCNTs incubated with human plasma proteins and free plasma were separated by 1D SDS-PAGE and analyzed with a long one-dimensional reversed phase liquid chromatography coupled mass spectrometry. More than 500 proteins were identified. Approximately 240 proteins were selected (see Figure 2) and grouped according to their physiological functions, and the donor-averaged relative abundances for the proteins in each (functional) group were calculated for PEG2-SWCNTs and free plasma.

some proteins in the PEG2-SWCNTs' coronas were enriched/depleted with respect to their physiological relative abundance upon adsorption onto some or all five the investigated PEG2-SWCNTs (Table S1 and Figure 3). These results showed that the binding of plasma proteins onto PEG2-SWCNTs did not simply correlate to their physiological relative abundances and may have important implications on the biocompatibility/toxicity profiles of PEG2-SWCNTs. The most striking examples were given by those proteins that were enriched/depleted with respect to their physiological relative abundance upon adsorption onto all five investigated PEG2-SWCNTs, thereby suggesting that the changes in relative abundance of these proteins due to nanotube adsorption did not correlate with either nanotube surface charge or PEG conformation. Albumin, the most abundant human plasma protein, was detected in low percentages on all the PEG2-SWCNTs (Figure 3L). Other examples of proteins that were depleted with respect to their physiological relative abundance upon nanotube adsorption were transport proteins (such as corticosteroid-binding protein, serotransferrin, vitamin D-binding protein, ceruloplasmin, and hemopexin, Figure 3G) and acute phase reactants (such as α-1-antitrypsin and α-1-antichymotrypsin, Figure 3H), whereas examples of proteins that were enriched with respect to their physiological relative abundance upon nanotube adsorption were the Ig μ chain C region (Figure 3C) and all of the components of the molecular C1 complex (C1q, C1r, and C1s, Figure 3E).

In order to understand the relationship between specific properties of PEG2-SWCNTs and changes in protein adsorption, we next investigated the differences in relative abundance of plasma proteins among pairs of coronas adsorbed onto PEG2-SWCNTs differing in only one physicochemical property (surface charge or PEG conformation) (Table 2, Figure 4, and Figure S2). In particular, we focused our attention on two of the major components of the PEG2-SWCNTs' coronas (HFG and Ig). HFG (fibrinogen or coagulation factor I) is a hexameric ($\alpha_2\beta_2\gamma_2$) ~405 kDa molecular weight glycoprotein that is synthesized in the liver by hepatocytes and participates in blood clot formation as a fibrin precursor. The protein has a filamentous sigmoid-like shape with a length of ~48 nm and a diameter of ~6 nm and is negatively charged at physiological pH (pI = 5.5) (Table S2). There were no statistically significant differences in the relative abundance of HFG among the coronas of cPEG2-SWCNT-a, cPEG2-SWCNT-m, and cPEG2-SWCNT-750, whereas the abundance of HFG in the coronas of fPEG2-SWCNT-m and fPEG2-SWCNT-750 was ~5 and ~4 times higher than that in the coronas of cPEG2-SWCNT-m and cPEG2-SWCNT-750, respectively (Figure 4A). Immunoglobulins are globular glycoprotein molecules that play an essential role in the immune system. On the basis of differences in the amino acid sequence in the constant region of the heavy chains, Ig are divided into classes (or isotypes) that have different concentrations in serum (in the order IgG > IgA > IgM > IgD > IgE), have diverse structures and properties, and carry out different functions (Table S2). The relative abundance for IgA, IgG, and IgM in the PEG2-SWCNTs' coronas was calculated by summing the relative abundance values for Ig α, γ, and μ chains (C region), respectively (Figure 4A). IgG formed similar fractions for all of the PEG2-SWCNTs' coronas, whereas the fraction in the coronas of cPEG2-SWCNT-m and cPEG2-SWCNT-750 formed by IgM was ~3 and ~2 times higher than that in the coronas of fPEG2-SWCNT-m and fPEG2-SWCNT-750, respectively. The fraction in the corona of cPEG2-SWCNT-m formed by IgA was ~17 times higher than that in the corona of fPEG2-SWCNT-m. There was no statistical difference in the relative abundance of IgA and IgM among the cPEG2-SWCNTs' and fPEG2-SWCNTs' coronas.

TABLE 2. Proteins of the PEG2-SWCNTs' Coronas That Showed Statistical Differences among Pairs of PEG2-SWCNTs Differing in Only One Physicochemical Property[a]

		surface charge				PEG density	
group	protein	1 *vs* 2	2 *vs* 3	1 *vs* 3	4 *vs* 5	2 *vs* 4	3 *vs* 5
coagulation	fibrinogen					↑	↑
	α-2-macroglobulin	↓			↑	↓	
	factor XI					↑	↑
	factor XII					↑	
	plasminogen					↑	↑
	kininogen (HMW+LMW)					↑	↑
	vitronectin	↑			↓	↑	↑
	prothrombin					↑	
	kallikrein					↑	↑
	histidine-rich glycoprotein	↑			↓	↑	↑
immunoglobulin	IgA					↓	
	IgM					↓	↓
apolipoproteins	ApoA-I					↓	↓
	ApoA-IV				↓		
	ApoC-III				↑	↑	
	ApoC-IV						↓
	β-2-glycoprotein 1 (ApoH)					↑	↑
	clusterin (ApoJ)				↓	↑	↑
complement	C1q (a+b+c subunit)					↓	↓
	C1r					↓	
	C1s					↓	
	C3	↑				↓	↓
	C5		↓				
	C6C	↑	↓			↓	
	C7	↑	↓		↑	↓	
	C8	↑				↓	
	C9	↑	↓			↓	↓
complement (factors)	Factor H	↑				↑	↑
	Factor-H-related protein 1					↑	↑
	C4 binding protein (α+β chain)					↓	
transport	cholesteryl ester transfer protein					↑	↑
	hemopexin			↑			↑
acute phase	inter-α-trypsin inhibitor H4		↓			↑	↑
	lipopolysaccharide binding protein					↑	↑
other components	haptoglobin-related protein					↓	
	gelsolin					↑	↑
	pregnancy zone protein				↑		
	galectin-3-binding protein				↑	↓	
	protein AMBP		↑	↑			↓
	inter-α (globulin) inhibitor H2						↑

[a] Statistical analysis (non-parametric Mann−Whitney U statistic) among pairs of PEG2-SWCNTs differing in surface charge or PEG density. We used arrows to indicate the statistical changes (increases or decreases) in protein amounts with varying the physicochemical properties of PEG-SWCNTs (↓ or ↑ $0.01 < p \leq 0.05$). For brevity: 1 = cPEG2-SWCNT-a; 2 = cPEG2-SWCNT-m; 3 = cPEG2-SWCNT-750; 4 = fPEG2-SWCNT-m; 5 = fPEG2-SWCNT-750.

We also investigated the enrichment/depletion among IgM *versus* IgG, IgM *versus* HFG, and IgG *versus* HFG upon adsorption onto PEG2-SWCNTs with respect to the physiological values (Figure 4C). We did not consider the IgA isotype in our analysis because the DPSC values calculated for IgA were dispersed and it made it difficult to compare the enrichment/depletion of IgA with respect to the other Ig isotypes and HFG. IgM/IgG DPSC ratios were higher than the physiological value for all of the PEG2-SWCNTs. The analysis of the Ig/HFG DPSC ratios for the IgM and IgG isotype showed that the IgM/HFG ratio was higher than the physiological value for cPEG2-SWCNTs, whereas it was lower than the physiological value for fPEG2-SWCNTs. IgG/HFG DPSC ratio was statistically different (lower) with respect to the physiological value only for fPEG2-SWCNTs. Taken together, these data suggested that the order of adsorption of HFG, IgM, and IgG was IgM > HFG = IgG for cPEG2-SWCNTs and HFG > IgM > IgG for fPEG2-SWCNTs.

Finally, we found that 40 proteins (including HFG, IgM, and IgA) showed different relative abundances

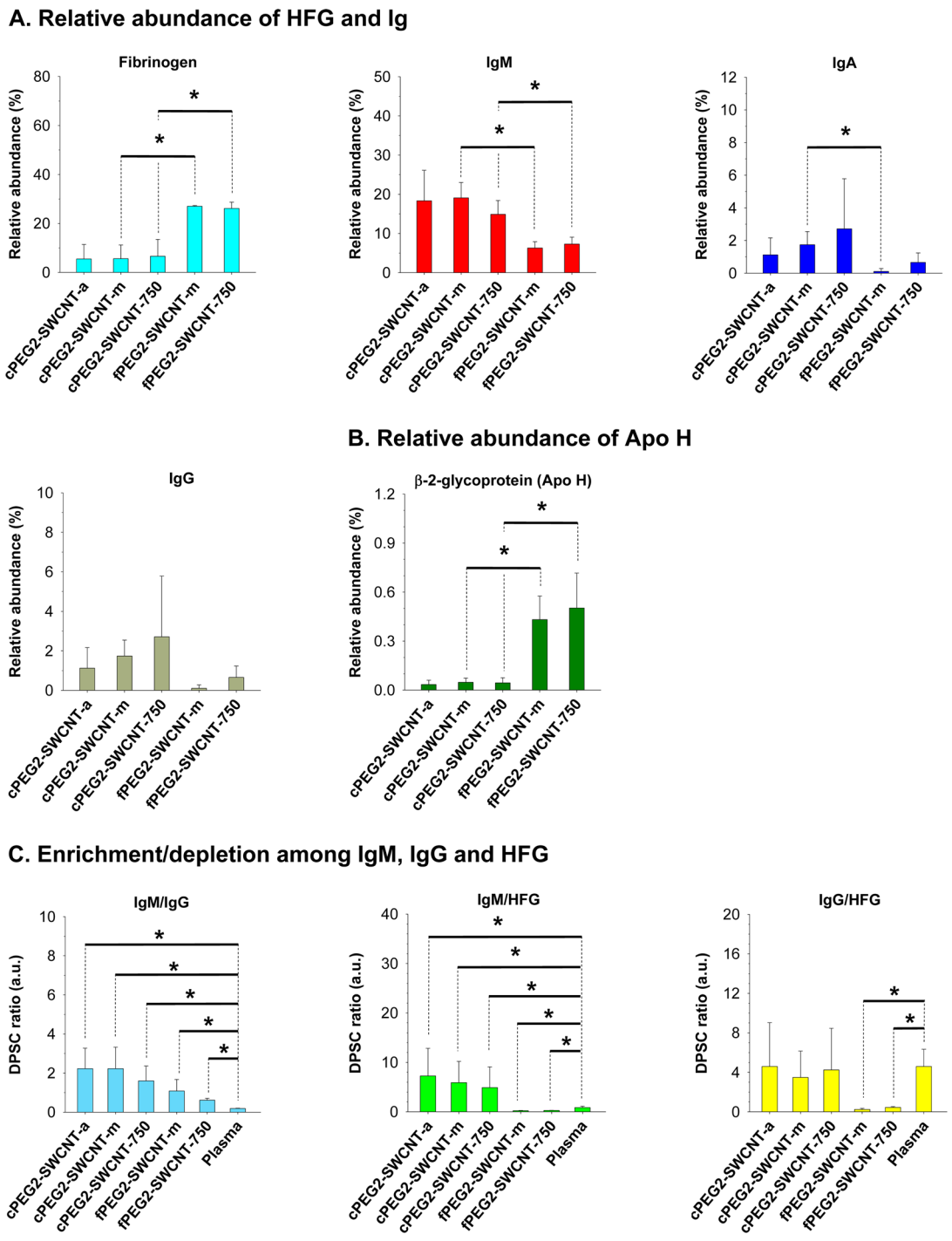

Figure 4. Statistical analysis (nonparametric Mann−Whitney U statistic). (A) Relative abundance of two of the major components (HFG and Ig) in the PEG2-SWCNTs' coronas. (B) Relative abundance of β-2-glycoprotein (Apo H) in the PEG2-SWCNTs' coronas. (C) DPSC ratios among IgM, IgG, and HFG in the PEG2-SWCNTs' coronas and plasma; *$0.01 < p \leq 0.05$.

among the PEG2-SWCNTs' protein coronas, mostly due to changes in PEG conformations (Table 2 and Figure S2). Indeed, only three proteins (Apo A-IV, complement C5, and pregnancy zone protein) showed different relative abundances exclusively due to changes in the surface charge of PEG2-SWCNTs, whereas 22 proteins showed different relative abundances exclusively due to changes in PEG conformation. It is worth noting that β-2-glycoprotein (Apo H) showed relative abundances in the coronas of fPEG2-SWCNT-m and fPEG2-SWCNT-750 10 times higher than those in the coronas of cPEG2-SWCNT-m and cPEG2-SWCNT-750, respectively (Figure 4B). The latter result may have implications for the different biodistribution profiles exhibited by cPEG2-SWCNT-750 and fPEG2-SWCNT-750 as discussed below.

Biodistribution of PEG2-SWCNTs. Despite the limitations imposed by the fact that the above-mentioned

experiments were carried out *in vitro*—thereby not taking into account the effects of blood cells, platelets, and microparticles—and that information about the "soft" corona was not collected, we wondered whether variations in the PEG2-SWCNTs' protein corona would correlate with their *in vivo* biological performance.

TABLE 3. Pharmacokinetic Parameters of cPEG2-SWCNT-750 and fPEG2-SWCNT-750[a]

sample	$T_{0.5\alpha}$ (h)	$T_{0.5\beta}$ (h)	AUC_∞ (h μg mL^{-1})	V_{SS} (mL)	C_L (mL h^{-1})
cPEG2-SWCNT-750	0.2	2.3	14.4	3.63	1.4
fPEG2-SWCNT-750	0.03	0.8	3.7	6.6	5.4

[a] Groups of three NOD mice were post-retro-orbitally given a single injection of 20 μg of either cPEG2-SWCNT-750 or fPEG2-SWCNT-750 in 100 μL of PBS. Blood samples were collected at different time points, and their near-infrared (NIR) emission was measured and used to obtain the pharmacokinetic parameters of PEG2-SWCNTs.

Twenty micrograms of cPEG2-SWCNT-750 and fPEG2-SWCNT-750 were administered to live mice, blood samples were collected, their NIR fluorescence was measured, and the pharmacokinetic parameters of PEG2-SWCNTs were calculated (Table 3). Both PEG2-SWCNTs displayed a biphasic (distribution−elimination) pharmacokinetic profile (Figure 5A). cPEG2-SWCNT-750 reached the distribution balance between blood and tissue in approximately 12 min and showed an eliminative half-life of ∼2 h. fPEG2-SWCNT-750 showed a very fast distribution time constant (∼2 min) and an eliminative half-life of ∼50 min, and exhibited a ∼4-fold faster clearance and a ∼2-fold larger steady-state volume of distribution than cPEG2-SWCNT-750.

Next, we analyzed the accumulation of PEG2-SWCNTs into organs 24 h following administration. Although the data yielded by this study were qualitative due to potential limitations related to the penetration

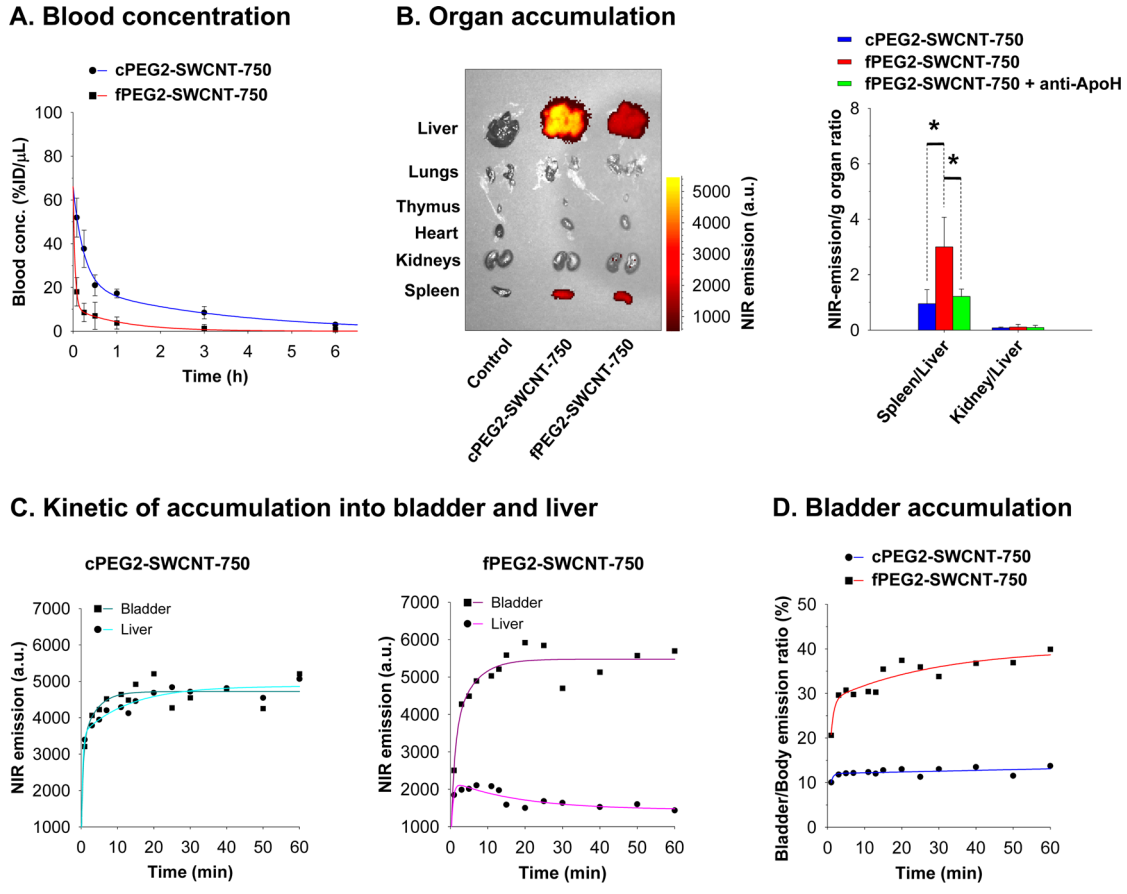

Figure 5. Biodistribution of cPEG2-SWCNT-750 and fPEG2-SWCNT-750. (A) Groups of three NOD littermate mice were given a single injection of 20 μg of either cPEG2-SWCNT-750 or fPEG2-SWCNT-750. Blood samples (approximately 100 μL) were collected at different time points, and their NIR emission was measured to calculate the concentration of PEG2-SWCNTs (%ID/μL) in the blood. (B) Groups of three NOD littermate mice were given a single injection of 20 μg of either cPEG2-SWCNT-750 or fPEG2-SWCNT-750. After 24 h, the mice were sacrificed, the organs were extracted and weighed, and the organs' NIR emission was measured. The average total NIR emission per gram of organ for spleen, liver, and kidneys was calculated, and the ratios between the values for any two organs are reported in the graph. Groups of three NOD littermate mice were depleted of Apo H by being twice administered 20 μg of rabbit anti-mouse Apo H mAbs 6 and 2 h before given a single injection of 20 μg of fPEG2-SWCNT-750. Nonparametric Mann−Whitney U statistic; *0.01 < $p \leq$ 0.05. (C,D) Groups of two CD1 littermate mice were retro-orbitally given a single injection of 20 μg of either cPEG2-SWCNT-750 or fPEG2-SWCNT-750, anesthetized, and the total NIR emission from liver and bladder was recorded during the first hour. NIR emission data from bladder and liver of a representative group of mice were fitted to a four-parameter exponential rise curve (C). NIR emission data from the bladder of a representative group of mice were also reported as percent of total body emission (D).

depth and scattering of NIR light in thick tissues, our measurements showed different patterns of organ accumulation for the two types of PEG2-SWCNTs (Figure 5B). Spleens from cPEG2-SWCNT-750- and fPEG2-SWCNT-750-treated mice showed similar average total NIR emissions, whereas livers from fPEG2-SWCNT-750-treated mice showed lower average total NIR emissions than livers from cPEG2-SWCNT-750-treated mice. Both PEG2-SWCNTs were detected in no or very low amounts in kidneys and other extracted organs (heart, lungs, and thymus) and were mostly found in the urine, thereby suggesting that they were mostly excreted *via* the renal route (data not shown).[34] We also calculated the average NIR emission per gram of organ for spleen, liver, and kidney as a qualitative measure of the density of nanoparticle organ accumulation. The ratios between these values suggested that cPEG2-SWCNT-750 accumulated in similar densities in spleen and liver, whereas fPEG2-SWCNT-750 accumulated ~3-fold more densely in spleen than liver. Both PEG2-SWCNTs accumulated in much lower densities in the kidneys with respect to the liver (Figure 5B).

As we will discuss below, the differences in pharmacokinetic profiles exhibited by cPEG2-SWCNT-750 and fPEG2-SWCNT-750 could be explained by a combination of several factors such as nanoparticle physical properties (*i.e.*, aggregation), accessibility of adsorbed proteins by cell receptors, and differences in protein corona composition. It has been reported that some proteins, which are not traditionally considered as opsonins, could play a significant role in the clearance of nanoparticles by RES phagocytic cells. Chonn *et al.* have highlighted the involvement of Apo H in liposomal biodistribution.[35] In order to probe the role of Apo H on the biodistibution of PEG2-SWCNTs, we administered fPEG2-SWCNT-750 to mice whose serum had been transiently depleted of Apo H by following a protocol similar to that published by Chonn *et al.*[35] We have chosen fPEG2-SWCNT-750 because they showed higher relative abundance of Apo H than cPEG2-SWCNT-750 (Figure 4B). Groups of three mice received two injections of 20 μg of rabbit anti-mouse Apo H monoclonal antibodies (mAbs) in PBS or PBS alone (control) 6 and 2 h before being injected with a single dose (20 μg) of fPEG2-SWCNT-750. Depletion of Apo H from mAb-treated mouse serum was confirmed by Western Blot analysis (data not shown). Twenty four hours after nanotube injection, the mice were sacrificed, the organs were collected, and their NIR emission was recorded. The ratio between the values of average NIR emission per gram of organ for spleen and liver calculated for Apo H-devoid mice was ~2.5-fold lower than that obtained for control (non-Apo H-devoid) mice and suggested that the presence of Apo H in the PEG2-SWCNTs's protein corona may directly affect the relative spleen *versus* liver accumulation of PEG2-SWCNTs (Figure 5B).

Finally, in order to investigate differences among liver and renal clearances for the two types of PEG2-SWCNTs, mice were administered NIR-emitting PEG2-SWCNTs (10 μg), and the NIR emission from liver and bladder was recorded for 1 h in live anesthetized mice. The recorded profiles of NIR emission intensity showed accumulation of cPEG2-SWCNT-750 in both liver and bladder, whereas fPEG2-SWCNT-750 accumulated in the bladder but displayed an eliminative behavior following a short accumulative one in the liver (Figure 5C). These data suggested that fPEG2-SWCNT-750 entered the liver but were not uptaken by liver cells as efficiently as cPEG2-SWCNT-750 and were able, in part, to exit the organ. Furthermore, the total NIR emission from bladder was 40% of the total body NIR emission for fPEG2-SWCNT-750 1 h after administration and less than 15% for cPEG2-SWCNT-750 (Figure 5D). This observation suggested that fPEG2-SWCNT-750 was more efficiently cleared *via* the renal route than cPEG2-SWCNT-750.

DISCUSSION

Herein we investigated the effect of surface charge and PEG conformation of PEG2-SWCNTs on the protein corona and the biodistribution of the materials. PEG2-SWCNTs differing in surface charge and PEG conformation were fabricated and characterized (Figure 1). SWCNTs were modified with 2 kDa molecular weight PEG chains by either noncovalent (coating) or covalent (functionalization) techniques. We used AFM imaging to characterize the conformation of PEG chains onto PEG2-SWCNTs. It has been reported that PEG-modified phospholipids randomly adsorb onto surfaces, thereby leaving open areas as well as congested ones.[36] Our AFM data suggested a similar behavior for PEG-modified phospholipids while adsorbing onto SWCNTs. We found that the noncovalent process of PEGylation was not able to uniformly modify the sidewalls of SWCNTs with PEG chains, and more than half of the cPEG2-SWCNTs showed exposed portions of the unmodified SWCNT sidewall extending for several tens of nanometers (Figure 1C). On the other hand, covalent amidation of oxidized nanotubes was able to produce a denser and uniform PEG-modification on the sidewalls of SWCNTs than noncovalent adsorption of PEG-modified phospholipids (Figure 1F). However, we found that a small fraction (less than 10%) of fPEG2-SWCNTs showed portions of unmodified SWCNT sidewall. This result suggested that amidation was also unable to completely cover nanotube sidewalls with PEG chains, probably because of the insufficient and/or nonuniform spatial distribution of the carboxylic groups generated through oxidation.[37,38]

The goal of this study was to identify the proteins in the protein coronas adsorbed onto PEG-modified

nanotubes and assess differences in protein relative abundance due to changes in nanoparticle physical properties. We identified the plasma proteins adsorbed onto PEG2-SWCNTs by means of LC/MS/MS. Label-free relative quantification of plasma proteins adsorbed onto nanotubes was performed using differential protein spectral count analysis of proteins identified from SDS-PAGE gel. Although it is not a truly quantitative technique, label-free differential proteomics analysis based on peptide/protein spectral count using technical and biological replicates yielded to robust "semi-quantitative" relative abundance data. Statistical analysis (non-parametric Mann−Whitney U statistic) on pairs of coronas adsorbed onto PEG2-SWCNTs differing in only one property was performed in order to correlate differences in protein relative abundance to specific properties of PEG2-SWCNTs while avoiding artifacts caused by proteome variability. Although several studies have been conducted to identify the protein corona bound by different types of nanoparticles and the mechanisms regulating the amount/repertoire of adsorbed proteins, they were mainly based on nonstatistical analyses and on single or technical replicates.[29,39,40] Only few recent studies have statistically approached the problem.[41−43] Technical replicate-based analyses are important to assess the reliability of the assays used (Figure S4), but the robustness of the conclusions drawn about the amounts of adsorbed proteins might be affected by proteome variability among individuals.

Our data showed that PEG modification did not abrogate the adsorption of plasma proteins onto SWCNTs. This result, along with other recent studies about PEG-modified spherical nanoparticles,[8−10] contradicts the general idea that PEG modification forms a surface-random cloud that abrogates the adsorption of the protein corona onto nanoparticles. Furthermore, we found that the pattern of adsorbed proteins was affected by the conformation of PEG more than nanoparticle charge (Table 2 and Figure S2). A change in surface PEG conformation on SWCNT sidewalls from mushroom to mushroom-brush transition affected the relative content of two of the major components of the PEG2-SWCNTs' corona (HFG and Ig, Figures 4 and S2). The order of adsorption of HFG and Ig was IgM > HFG = IgG for PEG2-SWCNTs with PEG in mushroom configuration (cPEG2-SWCNTs) and HFG > IgM > IgG for PEG2-SWCNTs with PEG in mushroom-brush transition configuration (fPEG2-SWCNTs). In a recent investigation carried out using single protein solutions, Ge *et al.* have reported that the adsorption of bovine fibrinogen (BFG) and IgG onto pristine SWCNTs was competitive with an order BFG > IgG and driven by $\pi-\pi$ stacking interactions.[44] The amount of adsorbed proteins positively correlated with the surface (and total) number of hydrophobic residues (in particular Tyr, Phe, and Trp). However, the orders of adsorption of BFG *versus* IgM and IgM *versus* IgG onto SWCNTs were not investigated. The order of adsorption for HFG, IgM, and IgG onto PEG2-SWCNTs did not correlate with protein hydrophobicity for either cPEG2-SWCNTs or fPEG2-SWCNTs, thereby suggesting that other protein properties influenced the adsorption of these major corona components (Table S2). The fact that, although carrying a lower number of hydrophobic residues, HFG adsorbed onto fPEG2-SWCNTs more efficiently than IgM (Figure 4C) suggests that the filamentous shape of HFG possibly allows it to more efficiently reach the graphitic sidewall through the dense PEG cloud when compared to IgM, which has a planar shape. In other words, a change in surface PEG conformation from mushroom to mushroom-brush transition might change the adsorption of the plasma proteins HFG and IgM onto PEG2-SWCNTs from an hydrophobicity-driven process to a more shape-driven one. This is certainly a preliminary model and does not perfectly fit the adsorption of other proteins. For instance, this model does not explain the fact that, although characterized by higher hydrophobicity, HFG did not adsorb onto cPEG2-SWCNTs with higher efficiency than IgG (Figure 4). Other variables that may originate from either direct or indirect actions of PEG on protein adsorption should be considered. We cannot rule out that certain plasma proteins could directly interact with PEG chains. It has been hypothesized that PEG chains, although lacking defined chemical groups promoting direct recognition, may drive the recruitment of complement activator complexes onto PEG-modified SWCNTs.[45] A direct interaction of HFG with PEG chains would explain the higher amount of HFG on fPEG2-SWCNTs with respect to cPEG2-SWCNTs (Figure 4A). However, it is also possible that PEG may indirectly affect protein adsorption through water activity. It is well-established that PEG chains cluster water molecules and can affect the hydration (and conformational) state of proteins adsorbed onto PEG-modified surfaces. A "C3 tickover" due to conformational changes following adsorption onto PEG-modified SWCNTs has been reported.[46] Similarly, HFG hydration and the following conformational changes and aggregation may become accelerated upon adsorption onto densely PEG-modified SWCNTs. Conformational changes of HFG upon adsorption onto nanoparticles and its effects on nanoparticles toxicity have been described.[47]

Our statistical analysis showed that a total of 40 proteins exhibited different relative abundances among the PEG2-SWCNTs' protein coronas mostly due to changes in PEG conformation (Table 2 and Figure S2). However, our investigation was based on SWCNTs modified with 2 kDa molecular weight linear PEG chains. Preliminary investigations about the protein corona adsorbed onto SWCNTs modified with 2 and 5 kDa molecular weight PEG chains following

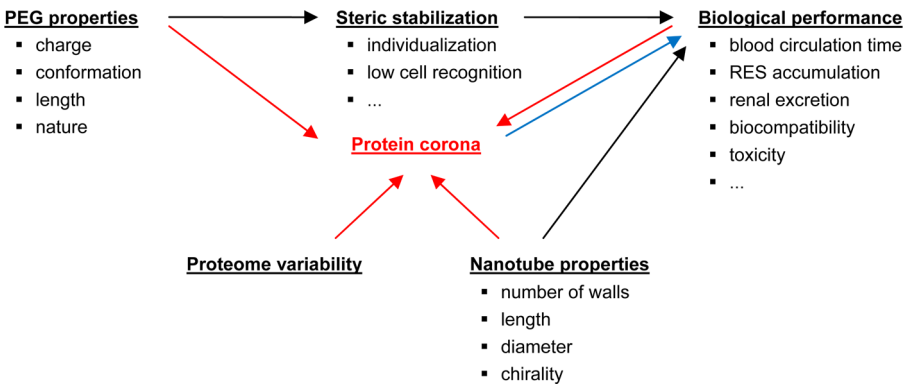

Figure 6. Hypothesized role of protein corona in the biological performance of PEG-modified SWCNTs. The biological performance of PEG-modified SWCNTs has been traditionally thought to be influenced by nanotube properties and steric stabilization, which is driven by PEG properties (black arrows). Immediately after the administration of PEG-modified SWCNTs *in vivo*, plasma proteins start adsorbing onto the nanoparticles. The process of protein corona formation onto PEG-modified SWCNTs is dynamic and governed by both nanotube and PEG properties, proteome variability, and the biological performance of PEG-SWCNTs (*i.e.*, the local and temporal blood concentration of nanotubes) (red arrows). Our data suggest that protein corona repertoire, along with steric stabilization and nanotube properties, may mediate the action of PEG conformation on the biological performance PEG-SWCNTs (blue arrow).

incubation with human plasma at 4 °C for 1 h (Table S3 and Figures S5 and S6) suggested that, along with conformation, PEG length may play an important role in the formation of the PEG-SWCNTs' protein corona. Although a comprehensive analysis of the protein corona adsorbed onto PEG-SWCNTs at 4 °C is beyond the scope of this article, it is worth describing a couple of results. HFG and IgM showed statistically significant different relative abundances between the cPEG2-SWCNT-m's and fPEG2-SWCNT-m's protein coronas, whereas their relative abundances were similar between the cPEG5-SWCNT-m's and fPEG5-SWCNT-m's coronas (Figure S7A). The order of adsorption of HFG and IgM was IgM > HFG for cPEG2-SWCNTs and HFG > IgM for fPEG2-SWCNTs, whereas HFG and IgM adsorbed with similar efficiency onto cPEG5-SWCNTs and fPEG5-SWCNTs (Figure S7B). Gref *et al.* have reported that both PEG length and surface density influence the protein corona of PEG-modified polymeric nanoparticles.[10] Our results suggested that, by increasing PEG length, the effect of PEG conformation on the adsorption of HFG and IgM onto PEG-SWCNTs becomes weaker. A clear explanation of this phenomenon is still missing, and more investigations about the protein corona of SWCNTs modified with PEG chains having different lengths (as well as nature, *i.e.*, linear *versus* branched) are warranted in order to shed light on the interplay of PEG properties on the adsorption of plasma proteins onto PEG-SWCNTs.

Finally, we investigated the effects of PEG conformation on the biodistribution of PEG2-SWCNTs. Our data showed that a change in PEG conformation from mushroom to mushroom-brush transition led to shorter blood circulation time, faster renal clearance, and higher spleen *versus* liver accumulation of PEG2-SWCNTs (Figure 5). Since AFM imaging showed that both the PEG2-SWCNTs used in the experiments had a transverse dimension well below the diameter of renal fenestra (~30 nm), the fact that cPEG2-SWCNTs and fPEG2-SWCNTs showed different renal excretion efficiencies could be explained by differences in the level of aggregation of PEG2-SWCNTs as soon as they enter the bloodstream. It is likely that fPEG2-SWCNTs were able to remain as individual nanoparticles for a longer duration of their blood circulation by virtue of their dense PEG coating, whereas cPEG2-SWCNTs had a tendency to form bundles that were less prone to cross the glomerular filter than fPEG2-SWCNTs. Recently, Lacerda *et al.* have pointed out that individualization, along with dimension, shape, and structural characteristics (*i.e.*, charge), is pivotal to enable efficient clearance of nanoparticles through the renal route.[22,23] The authors showed that highly individualized carbon nanotubes with length considerably larger than the glomerular pores can be efficiently excreted through the renal route with low accumulation in the liver. The observed differences in the spleen *versus* liver accumulation of PEG2-SWCNTs might be correlated to other mechanisms, along with differences in the level of aggregation of PEG2-SWCNTs. First, the higher PEG density of fPE2-SWCNTs *versus* cPEG2-SWCNTs could prevent receptor-mediated recognition by (liver) phagocytic cells of certain plasma proteins equally adsorbed onto both cPEG2-SWCNTs and fPEG2-SWCNTs (*i.e.*, IgG).[6,7] Second, quantitative differences in the presence of certain plasma proteins in the PEG2-SWCNTs' protein corona may be responsible for differences in biodistribution. For example, the higher amounts of IgM adsorbed onto cPEG2-SWCNTs could be responsible for their higher liver accumulation than fPEG2-SWCNTs. Other proteins, which preferentially adsorbed onto fPEG2-SWCNTs with respect to cPEG2-SWCNTs (Table 2 and Figure S2), are not traditionally considered as opsonins but could still drive the accumulation of fPEG2-SWCNTs in the RES organs. For

example, it has been described that the adsorption of vitronectin and β-2-glycoprotein (Apo H) onto nanoparticles plays a significant role in the clearance of nanoparticles by RES phagocytic cells.[30,35] We probed the effect of the transient depletion of Apo H from mouse plasma on the organ accumulation of fPEG2-SWCNT-750. This investigation showed that Apo H depletion causes a decrease in the relative spleen *versus* liver uptake of fPEG2-SWCNT-750. Although a clear picture of the regulatory mechanisms of this phenomenon is still missing, our data suggest that the presence of Apo H in the PEG2-SWCNTs' protein corona may directly influence the biodistribution of PEG2-SWCNTs (Figure 5).

CONCLUSIONS

Here, for the first time, we report a study about the effects of surface charge and PEG conformation on the pattern of plasma protein adsorbed onto PEG2-SWCNTs and the effects of PEG conformation on the biodistribution of PEG2-SWCNTs. Our investigation led to several results. First, we showed that the recruitment of plasma proteins onto PEG2-SWCNTs is independent from the isoelectric point, molecular weight, total hydrophobicity, and number of polyaromatic residues of the proteins. Second, statistical analysis of the relative abundance of plasma proteins among the PEG2-SWCNTs' coronas showed that several plasma proteins were enriched/depleted upon adsorption onto PEG2-SWCNTs with respect to their physiological relative abundance independent of nanotube surface charge and PEG conformation. Third, statistical analysis on the relative abundance of plasma proteins in the PEG2-SWCNTs' coronas showed that PEG conformation had a deeper influence on the composition of the protein corona compared to nanotube surface charge. In particular, PEG conformation affected the adsorption of the corona's major constituents. This result suggests that PEG conformation also influences the protein properties driving the adsorption onto PEG2-SWCNTs. Finally, *in vivo* investigations showed that PEG conformation affected the biodistribution of PEG2-SWCNTs and suggested that the adsorption of certain proteins may directly influence the biodistribution of PEG2-SWCNTs.

Nanoparticle physical properties (dimension, shape, and structural characteristics) and the type of chemical modification (*i.e.*, PEG density, charge, length, and nature) traditionally are believed to affect nanoparticle biological performance mainly through effects on nanoparticle aggregation and accessibility for ligation to receptors on phagocytic cells. The protein corona has recently emerged as another key determinant of the biological performance of nanoparticles at both the cellular and whole animal level.[13] Our study is the first to address the protein corona of PEG-modified SWCNTs and suggests a causal relationship between surface PEG conformation, pattern of adsorbed plasma protein, and pharmacokinetic profile of PEG-modified SWCNTs (Figure 6).

MATERIALS AND METHODS

Fabrication of PEG(2k)-Coated SWCNTs (cPEG2-SWCNT-a, cPEG2-SWCNT-m, and cPEG2-SWCNT-750). cPEG2-SWCNT-a were fabricated through the adsorption of 1,2-distearoyl-*sn*-glycero-3-phosphoethanolamine-*N*-[amino(polyethylene glycol)-2000] (Avanti Polar Lipids, Inc., Alabaster, AL) onto SWCNT sidewalls. First, 5 mg of oven-dried pristine (nonfunctionalized) SWCNTs (Carbon Solutions, Inc., Riverside, CA) were sonicated with phospholipids (25 mg) in PBS for 6 h by an ultrasonic bath (Cole-Parmer, Vernon Hills, IL). The temperature of the water in the bath was maintained at ~20 °C. Next, the mixture was fractionated by stepwise centrifugation to isolate short hydrophilic amino-terminated PEG(2k)-coated SWCNTs and washed eight times through 100 kDa cutoff filters in Milli-Q H_2O (Amicon Ultra, Millipore, Billerica, MA) to remove free phospholipids. cPEG2-SWCNT-m were fabricated by incubating cPEG2-SWCNT-a with methyl-terminated short poly(ethylene oxide) chains carrying an activated carboxylic group (NHS-mPEO, Thermo Scientific, Rockford, IL) overnight (o/n) at room temperature and following washing through 100 kDa cutoff filters in Milli-Q H_2O. For *in vivo* experiments, PEG(2k)-coated SWCNTs carrying near-infrared (NIR)-emitting fluorochromes were fabricated by incubating cPEG2-SWCNT-a with 750 nm emitting fluorochromes carrying activated carboxyl groups (NHS-Seta750, ex 752 nm/em 778 nm, SETA BioMedicals, Urbana, IL) o/n in the dark at room temperature and purified by filtration on 100 kDa cutoff filters in Milli-Q H_2O. The fluorochrome was chosen in order to minimize the background noise arising from tissue autofluorescence.

Fabrication of PEG(5k)-Coated SWCNTs (cPEG5-SWCNT-a and cPEG5-SWCNT-m). PEG(5k)-coated SWCNTs were fabricated by using 1,2-distearoyl-*sn*-glycero-3-phosphoethanolamine-*N*-[amino-(polyethylene glycol)-5000] (Nanocs, Boston, MA) and following a protocol similar to that described for PEG(2k)-coated SWCNTs.

Fabrication of PEG(2k)-Functionalized SWCNTs (fPEG2-SWCNT-a, fPEG2-SWCNT-m, and fPEG2-SWCNT-750). fPEG2-SWCNT-a were fabricated by incubating 3 mg of oven-dried carboxylic acid-functionalized SWCNTs (Carbon Solutions) with 100 mg of α-amino-ω-Boc-amino PEG(2 kDa) (Rapp Polymere GmbH, Tuebingen, Germany) in 10 mL of dichloromethane (DCM) containing 125 μL of 1 M *N*,*N*′-dicyclohexylcarbodiimide and 60 mg of 4-dimethylaminopyridine (Sigma-Aldrich, St. Louis, MO). The amidation reaction was carried out for 48 h under constant sonication by means of an ultrasonic bath. The temperature of the water in the bath was maintained at ~20 °C. The mixture was dried under vacuum, resuspended in 5 mL of Milli-Q H_2O, centrifuged at 100 000*g* for 3 h at 4 °C, and purified by filtration. Boc was unprotected by using a trifluoroacetic acid (TFA) solution 1:1 (v/v) in DCM. fPEG2-SWCNT-m were fabricated by incubating fPEG2-SWCNT-a with NHS-mPEO o/n at room temperature and following by washing through 100 kDa cutoff filters in Milli-Q H_2O. For *in vivo* experiments, we fabricated fPEG2-SWCNT-750 by incubating fPEG2-SWCNT-a with NHS-Seta750 o/n in the dark at room temperature and purified by filtration on 100 kDa cutoff filters in Milli-Q H_2O.

Fabrication of PEG(5k)-Functionalized SWCNTs (fPEG5-SWCNT-a and fPEG5-SWCNT-m). PEG(5k)-functionalized SWCNTs were fabricated by using α-amino-ω-Boc-amino PEG(5 kDa) (Rapp Polymere GmbH) and following a protocol similar to that described for PEG(2k)-functionalized SWCNTs.

AFM Imaging of PEG-SWCNTs. A few microliters of amino-terminated PEG-SWCNTs in PBS were dropped onto a freshly

cleaved mica substrate (Ted Pella, Redding, CA) and allowed to stand for a couple of minutes. The mica surface was rinsed with water and dried under a gentle nitrogen stream. AFM images were recorded through an 5500 AFM (Agilent Technologies, Inc., Santa Clara, CA).

Calculation of PEG Density of PEG-SWCNTs. The values of PEG density were obtained by calculating the concentration of both amino groups on amino-terminated PEG-SWCNTs by Kaiser test and fluorochromes on Seta750-conjugated PEG-SWCNTs by our published protocol.[17]

Dynamic Light Scattering. The surface charges of PEG-SWCNTs were recorded by means of a Zetasizer NanoZS (Malvern, Worcestershire, UK) as described elsewhere.[48−50] Measurements were performed at 25 °C using 0.1 mg/mL PEG-SWCNT solutions in both Milli-Q H_2O and PBS.

Pharmacokinetic of cPEG2-SWCNT-750 and fPEG2-SWCNT-750. The animal work described in this article was carried out at the La Jolla Institute for Allergy and Immunology (LIAI) and approved by the LIAI IACUC (AP140-NB4-0610). All efforts were made to minimize animal suffering. Groups of three NOD mice (The Jackson Laboratory, Bar Harbor, MA) were retro-orbitally given a single injection of 20 μg of either cPEG2-SWCNT-750 or fPEG2-SWCNT-750 in 100 μL of PBS. Control mice were injected with PBS. Blood samples (~100 μL) were collected from the saphenous vein at different time points and centrifuged at 1300*g* at 4 °C for 10 min to pellet the red and white cells. Supernatants were collected, and their NIR emission was measured by means of a Xenogen IVIS imager (PerkinElmer, Waltham, MA). The NIR emission of control mice blood samples was subtracted from that of treated mice blood samples. The percent injected dose of PEG2-SWCNTs per microliter of blood (% ID/μL) was calculated by calibrating NIR emission of PEG2-SWCNTs in the blood. The fluorescence of cPEG2-SWCNT-750 and fPEG2-SWCNT-750 was calibrated by mixing equal volumes of mouse plasma with different concentrations of nanotubes and recording the NIR emission. NIR emission of both nanoparticles showed a linear dependence with nanoparticle concentration in the range of interest (from 0.1 to 10 mg/L, Figure S3). The obtained values were best fitted by using a two-compartmental model ($R = 1$), and the plasma pharmacokinetic parameters of PEG-SWCNTs were obtained.

Organ Accumulation of cPEG2-SWCNT-750 and fPEG2-SWCNT-750. Groups of three NOD mice were retro-orbitally administrated with a single injection of 20 μg of either cPEG2-SWCNT-750 or fPEG2-SWCNT-750 in 100 μL of PBS. Control mice were injected with PBS. After 24 h, mice were sacrificed by CO_2 asphyxiation, the organs extracted and weighed, and the organs' NIR emission was measured with a Xenogen IVIS imager. The average total NIR emission per gram of liver, spleen, and kidneys was calculated for both control and treated mice as a measure of the density of accumulation of PEG2-SWCNTs into organs. The density of accumulation of control organs was subtracted from those of treated mice and the obtained values used to calculate the ratio of density of accumulation between any two organs.

Effect of Apo H Depletion on Organ Accumulation of fPEG2-SWCNTs. Apo H was depleted from serum following a protocol similar to that published by Chonn *et al.*[35] Groups of three NOD mice were retro-orbitally injected twice with 20 μg of rabbit anti-mouse Apo H mAbs (Millipore) in PBS or PBS alone (control) 6 and 2 h before being injected with a single dose (20 μg) of fPEG2-SWCNT-750. Organ accumulation of fPEG2-SWCNT-750 was determined as described above.

Kinetic of Accumulation of cPEG2-SWCNT-750 and fPEG2-SWCNT-750 into Bladder and Liver. Groups of two CD1 littermate mice were retro-orbitally given with a single injection of 20 μg of either cPEG2-SWCNT-750 or fPEG2-SWCNT-750. Control mice were injected with PBS. Mice were anesthetized with a single intraperitoneal injection of 250 mg/kg Avertin solution, and the NIR emission from liver and bladder was recorded during the first hour by means of a Kodak In-Vivo FX. Avertin solution was prepared by mixing 0.5 mL of Avertin stock solution [25g Avertin (Sigma-Aldrich) in 15.5 mL of *tert*-amyl alcohol (Thermo Scientific)] with 39.5 mL of 0.9% saline. Accumulation kinetics of PEG2-SWCNTs into bladder and liver were calculated by subtracting the NIR emission of control organs from that of treated mice organs. Accumulation of PEG2-SWCNTs into the bladder was also calculated as a percent of total body emission by subtracting the NIR emission of control organs from that of treated mice organs and dividing by the total body NIR emission.

Human Plasma. Human blood was collected from three different anonymous healthy donors at the La Jolla Institute for Allergy & Immunology IRB-Approved Normal Blood Donors Program in heparin-coated tubes to prevent clotting. Blood was centrifuged at 1300*g* at 4 °C for 10 min to pellet the red and white cells. The supernatant (plasma) was aliquoted and stored at −80 °C until use. Defrosted plasma was centrifuged again at 1600*g* for 10 min before use to reduce the presence of degraded proteins.

Incubation with Plasma. Fifty micrograms of each PEG-SWCNT suspension in PBS was incubated for 1 h at 37 °C (or 4 °C) with 400 μL of human plasma in a final volume of 500 μL by adding PBS (80% final plasma concentration). The samples were washed four times in 500 μL of PBS by ultracentrifugation at 120 000*g* at 4 °C for 30 min, then the last pellets were resuspended in SDS sample buffer (62.5 mM Tris-HCl pH 6.8, 2% w/v SDS, 10% glycerol, 50 mM DTT, 0.01% w/v bromophenol blue) and boiled at 96 °C for 5 min. After a brief spin, the supernatants were run on a 4−20% Tris-glycine SDS-PAGE gel (Life Technologies, Grand Island, NY) and stained with SimplyBlue Safe Stain (Life Technologies) or with Pierce Silver Stain Kit (Thermo Scientific).

In-Gel Digestion and Sample Preparation for LC-MS/MS Analysis. Stained SDS-PAGE bands were cut into 1 mm × 1 mm pieces, transferred to a new EtOH-rinsed tube, destained by washing with 50% acetonitrile (ACN) in 50 mM ammonium bicarbonate, and vacuum-dried. Proteins were reduced with 5 mM dithiothreitol and alkylated with 15 mM iodoacetamide prior digestion by 25 ng/μL trypsin in 50 mM ammonium bicarbonate for 1 h on ice followed by additional 16 h at 37 °C under continuous shaking. Digested tryptic peptides were extracted from gels and transferred to a new tube. Three hundred microliters of HPLC grade H_2O was added, sonicated for 10 min, then the extracted peptides were added to the elution tube, following extraction by 5% formic acid (FA), four times with 50% ACN in 5% FA, once with 70% ACN, and finally with 100% ACN. Extracted peptides were all pooled together, vacuum-dried, and dissolved in 18 μL of 0.1% TFA. Tryptic peptides were then concentrated and desalted using a Millipore C18 Zip Tip (Millipore). The eluent was then vacuum-dried and dissolved in 32 μL of LC/MS loading buffer (2% ACN in 0.1% FA in Milli-Q H_2O).

Protein Identification Using LC/MS/MS. Eight microliters of Zip Tip-cleaned tryptic-digested samples was loaded to the automated Nano LC- LTQ MS/MS (Thermo Scientific, Waltham, MA), using an Eksigent Nano 2D LC system, a switch valve, a C18 trap column (Agilent, Inc., Santa Clara, CA), and a capillary reversed phase (RP) column (15 cm Magic C18 AQ resin, Bruker-Michrom Bioresources, Inc.) with an ADVANCE ESI source (Michrom) which is used to ionize the peptides while eluting from the RP column using a linear gradient elution from buffer A (2% ACN in Milli-Q H_2O plus 0.1% FA) to 15% buffer A plus 85% buffer B (ACN plus 0.1% FA) in 2 h. The LC/MS run was operated in the data-dependent mode. Data on the four strongest ions above an intensity of 50×10^4 were collected with dynamic exclusion enabled and collision energy set at 35%.

Protein Identification and Data Analysis. The MS/MS spectra were combined and analyzed by Sorcerer Enterprise v.3.5 release (Sage-N Research, Inc., Milpitas, CA) with SEQUEST algorithm as the search program for peptide/protein identification. SEQUEST was set up to search the target-decoy ipi.Human.v3.73 database containing protein sequences using trypsin for enzyme with the allowance of up to 2 missed cleavages, Semi Tryptic search and precursor mass tolerance of 1.5 atomic mass unit (amu). Differential search was performed to identify the following modifications: alkylation of cysteine residues, oxidation of methionine residues, phosphorylation of serine, threonine and tyrosine residues, lysine ubiquitination (by using GG or LRGG tags). The search results were viewed, sorted, filtered, and statically analyzed by using comprehensive proteomics data analysis software [Peptide/Protein prophet v.4.02 (Institute for Systems

Biology)]. In this study, we used the following two search criteria. First, the minimum trans-proteomic pipeline (TPP) probability score for proteins and peptides was set at 0.95 and 0.9, respectively, to ensure very low error [much less than a false discovery rate (FDR) of 2%] with reasonably good sensitivity. Second, we set the cross correlation (Xcorr) score threshold for filtered peptides equal to 1.5, 2.0, and 2.5 for 1, 2, and 3-charged fully digested peptides, respectively. Finally, the gene ontology analysis of identified protein and differential spectral count analysis were analyzed by QTools.[33]

Statistical Analysis. Nonparametric Mann–Whitney U analysis was performed by SPSS Statistics (IBM Corporation, Armonk, NY).

Conflict of Interest: The authors declare no competing financial interest.

Acknowledgment. This work was supported by a grant from the Arthritis National Research Foundation to M.B. and by LIAI Institutional funds to N.B. We thank G. Caldwell (Sanford Burnham Medical Research Institute, La Jolla, CA) and Dr. Stephanie Stanford (La Jolla Institute for Allergy and Immunology) for helpful comments.

Supporting Information Available: Additional statistical analysis of human plasma proteins adsorbed onto PEG2-SWCNTs; physical properties of the major components of the PEG2-SWCNTs' protein corona; PEG2-SWCNT NIR emission *vs* concentration calibration curve; physical properties of PEG(5k)-modified SWCNTs; reliability of DPSC values. This material is available free of charge *via* the Internet at http://pubs.acs.org.

REFERENCES AND NOTES

1. Riehemann, K.; Schneider, S. W.; Luger, T. A.; Godin, B.; Ferrari, M.; Fuchs, H. Nanomedicine—Challenge and Perspectives. *Angew. Chem., Int. Ed.* **2009**, *48*, 872–897.
2. Du, H.; Chandaroy, P.; Hui, S. W. Grafted Poly-(ethylene glycol) on Lipid Surfaces Inhibits Protein Adsorption and Cell Adhesion. *Biochim. Biophys. Acta* **1997**, *1326*, 236–248.
3. Needham, D.; McIntosh, T. J.; Lasic, D. D. Repulsive Interactions and Mechanical Stability of Polymer-Grafted Lipid Membranes. *Biochim. Biophys. Acta* **1992**, *1108*, 40–48.
4. Klibanov, A. L.; Maruyama, K.; Torchilin, V. P.; Huang, L. Amphipathic Polyethyleneglycols Effectively Prolong the Circulation Time of Liposomes. *FEBS Lett.* **1990**, *268*, 235–237.
5. Woodle, M. C.; Lasic, D. D. Sterically Stabilized Liposomes. *Biochim. Biophys. Acta* **1992**, *1113*, 171–199.
6. Blunk, T.; Hochstrasser, D. F.; Sanchez, J. C.; Müller, B. W.; Müller, R. H. Colloidal Carriers for Intravenous Drug Targeting: Plasma Protein Adsorption Patterns on Surface-Modified Latex Particles Evaluated by Two-Dimensional Polyacrylamide Gel Electrophoresis. *Electrophoresis* **1993**, *14*, 1382–1387.
7. Price, M. E.; Cornelius, R. M.; Brash, J. L. Protein Adsorption to Polyethylene Glycol Modified Liposomes from Fibrinogen Solution and from Plasma. *Biochim. Biophys. Acta* **2001**, *1512*, 191–205.
8. Dos Santos, N.; Allen, C.; Doppen, A. M.; Anantha, M.; Cox, K. A.; Gallagher, R. C.; Karlsson, G.; Edwards, K.; Kenner, G.; Samuels, L.; *et al.* Influence of Poly(ethylene glycol) Grafting Density and Polymer Length on Liposomes: Relating Plasma Circulation Lifetimes to Protein Binding. *Biochim. Biophys. Acta* **2007**, *1768*, 1367–1377.
9. Efremova, N. V.; Bondurant, B.; O'Brien, D. F.; Leckband, D. E. Measurements of Interbilayer Forces and Protein Adsorption on Uncharged Lipid Bilayers Displaying Poly-(ethylene glycol) Chains. *Biochemistry* **2000**, *39*, 3441–3451.
10. Gref, R.; Lück, M.; Quellec, P.; Marchand, M.; Dellacherie, E.; Harnisch, S.; Blunk, T.; Müller, R. H. `Stealth' Corona-Core Nanoparticles Surface Modified by Polyethylene Glycol (PEG): Influences of the Corona (PEG Chain Length and Surface Density) and of the Core Composition on Phagocytic Uptake and Plasma Protein Adsorption. *Colloids Surf., B* **2000**, *18*, 301–313.
11. Chonn, A.; Semple, S. C.; Cullis, P. R. Association of Blood Proteins with Large Unilamellar Liposomes *in Vivo*. Relation to Circulation Lifetimes. *J. Biol. Chem.* **1992**, *267*, 18759–18765.
12. Schreier, H.; Abra, R. M.; Kaplan, J. E.; Hunt, C. A. Murine Plasma Fibronectin Depletion after Intravenous Injection of Liposomes. *Int. J. Pharm.* **1987**, *37*, 233–238.
13. Monopoli, M. P.; Aberg, C.; Salvati, A.; Dawson, K. A. Biomolecular Coronas Provide the Biological Identity of Nanosized Materials. *Nat. Nanotechnol.* **2012**, *7*, 779–786.
14. Bottini, M.; Rosato, N.; Bottini, N. PEG-Modified Carbon Nanotubes in Biomedicine: Current Status and Challenges Ahead. *Biomacromolecules* **2011**, *12*, 338133–93.
15. Liu, Z.; Winters, M.; Holodniy, M.; Dai, H. siRNA Delivery into Human T Cells and Primary Cells with Carbon-Nanotube Transporters. *Angew. Chem., Int. Ed.* **2007**, *46*, 2023–2027.
16. Cato, M. H.; D'Annibale, F.; Mills, D. M.; Cerignoli, F.; Dawson, M. I.; Bergamaschi, E.; Bottini, N.; Magrini, A.; Bergamaschi, A.; Rosato, N.; *et al.* Cell-Type Specific and Cytoplasmic Targeting of PEGylated Carbon Nanotube-Based Nanoassemblies. *J. Nanosci. Nanotechnol.* **2008**, *8*, 2259–2269.
17. Delogu, L. G.; Stanford, S. M.; Santelli, E.; Magrini, A.; Bergamaschi, A.; Motamedchaboki, K.; Rosato, N.; Mustelin, T.; Bottini, N.; Bottini, M. Carbon Nanotube-Based Nanocarriers: The Importance of Keeping It Clean. *J. Nanosci. Nanotechnol.* **2010**, *10*, 5293–5301.
18. Prencipe, G.; Tabakman, S. M.; Welsher, K.; Liu, Z.; Goodwin, A. P.; Zhang, L.; Henry, J.; Dai, H. PEG Branched Polymer for Functionalization of Nanomaterials with Ultralong Blood Circulation. *J. Am. Chem. Soc.* **2009**, *131*, 4783–4787.
19. Yang, S. T.; Fernando, K. A.; Liu, J. H.; Wang, J.; Sun, H. F.; Liu, Y.; Chen, M.; Huang, Y.; Wang, X.; Wang, H.; *et al.* Covalently PEGylated Carbon Nanotubes with Stealth Character *in Vivo*. *Small* **2008**, *4*, 940–944.
20. Singh, R.; Pantarotto, D.; Lacerda, L.; Pastorin, G.; Klumpp, C.; Prato, M.; Bianco, A.; Kostarelos, K. Tissue Biodistribution and Blood Clearance Rates of Intravenously Administered Carbon Nanotube Radiotracers. *Proc. Natl. Acad. Sci. U.S.A.* **2006**, *103*, 3357–3362.
21. Schipper, M. L.; Nakayama-Ratchford, N.; Davis, C. R.; Kam, N. W.; Chu, P.; Liu, Z.; Sun, X.; Dai, H.; Gambhir, S. S. A Pilot Toxicology Study of Single-Walled Carbon Nanotubes in a Small Sample of Mice. *Nat. Nanotechnol.* **2008**, *3*, 216–221.
22. Lacerda, L.; Herrero, M. A.; Venner, K.; Bianco, A.; Prato, M.; Kostarelos, K. Carbon-Nanotube Shape and Individualization Critical for Renal Excretion. *Small* **2008**, *4*, 1130–1132.
23. Lacerda, L.; Soundararajan, A.; Singh, R.; Pastorin, G.; Al-Jamal, K. T.; Turton, J.; Frederik, P.; Herrero, M. A.; Li, S.; Bao, A.; *et al.* Dynamic Imaging of Functionalized Multi-Walled Carbon Nanotube Systemic Circulation and Urinary Excretion. *Adv. Mater.* **2008**, *20*, 225–230.
24. Liu, Z.; Davis, C.; Cai, W.; He, L.; Chen, X.; Dai, H. Circulation and Long-Term Fate of Functionalized, Biocompatible Single-Walled Carbon Nanotubes in Mice Probed by Raman Spectroscopy. *Proc. Natl. Acad. Sci. U.S.A.* **2008**, *105*, 1410–1415.
25. de Gennes, P. G. Conformation of Polymers Attached to an Interface. *Macromolecules* **1980**, *13*, 1069–1075.
26. Lee, J. H.; Lee, H. B.; Andrade, J. D. Blood Compatibility of Polyethylene Oxide Surfaces. *Prog. Polym. Sci.* **1995**, *20*, 1043–1079.
27. Steels, B. M.; Koska, J.; Haynes, C. A. Analysis of Brush-Particle Interactions Using Self-Consistent-Field Theory. *J. Chromatogr., B* **2000**, *743*, 41–56.
28. Stuart, C. Macromolecular Adsorption: A Brief Introduction. In *Biopolymers at Interfaces*; Marcel Dekker, Inc.: New York, 1998.
29. Cederwall, T.; Lynch, I.; Foy, M.; Berggard, T.; Donnelly, S. C.; Cagney, G.; Linse, S.; Dawson, K. A. Detailed Identification of Plasma Proteins Adsorbed on Copolymer Nanoparticles. *Angew. Chem., Int. Ed.* **2007**, *46*, 5754–5756.
30. Moore, A.; Weissleder, R.; Bogdanov, A., Jr. Uptake of Dextran-Coated Monocrystalline Iron Oxides in Tumor Cells and Macrophages. *J. Magn. Reson. Imaging* **1997**, *7*, 1140–1145.

31. Semple, S. C.; Chonn, A.; Cullis, P. R. Interactions of Liposomes and Lipid-Based Carrier Systems with Blood Proteins: Relation to Clearance Behaviour *in Vivo*. *Adv. Drug Delivery Rev.* **1998**, *32*, 3–18.
32. Cedervall, T.; Lynch, I.; Lindman, S.; Berggard, T.; Thulin, E.; Nilsson, H.; Dawson, K. A.; Linse, S. Understanding the Nanoparticle-Protein Corona Using Methods to Quantify Exchange Rates and Affinities of Proteins for Nanoparticles. *Proc. Natl. Acad. Sci. U.S.A.* **2007**, *104*, 2050–2055.
33. Brill, L. M.; Motamedchaboki, K.; Wu, S.; Wolf, D. A. Comprehensive Proteomic Analysis of *Schizosaccharomyces pombe* by Two-Dimensional HPLC-Tandem Mass Spectrometry. *Methods* **2009**, *48*, 311–319.
34. Although free fluorochromes were thoroughly washed away from nanoparticle solutions, we could not rule out the presence of free fluorochromes in cPEG2-SWCNT-750 and fPEG2-SWCNT-750 solutions. However, preliminary investigations had shown that NIR-emitting fluorochromes in free form, conjugated to PEG chains or conjugated to PEG-modified phospholipids, were excreted through urine without accumulating in any organs when administered to mice in amounts equivalent to those conjugated to 20 μg of cPEG2-SWCNT-750 and fPEG2-SWCNT-750 (data not shown). These data suggested that the observed organ NIR emission almost exclusively arose from the nanotubes.
35. Chonn, A.; Semple, S. C.; Cullis, P. R. Beta 2 Glycoprotein I Is a Major Protein Associated with Very Rapidly Cleared Liposomes *in Vivo*, Suggesting a Significant Role in the Immune Clearance of "Non-Self" Particles. *J. Biol. Chem.* **1995**, *270*, 25845–25849.
36. Du, H.; Chandaroy, P.; Hui, S. W. Grafted Poly-(ethylene glycol) on Lipid Surfaces Inhibits Protein Adsorption and Cell Adhesion. *Biochim. Biophys. Acta* **1997**, *1326*, 236–248.
37. Liu, J.; Rinzler, A. G.; Dai, H.; Hafner, J. H.; Bradley, R. K.; Boul, P. J.; Lu, A.; Iverson, T.; Shelimov, K.; Huffman, C. B.; *et al.* Fullerene Pipes. *Science* **1998**, *280*, 1253–1256.
38. Ziegler, K. J.; Gu, Z.; Peng, H.; Flor, E. L.; Hauge, R. H.; Smalley, R. E. Controlled Oxidative Cutting of Single-Walled Carbon Nanotubes. *J. Am. Chem. Soc.* **2005**, *127*, 1541–1547.
39. Lundqvist, M.; Stigler, J.; Elia, G.; Lynch, I.; Cedervall, T.; Dawson, K. A. Nanoparticle Size and Surface Properties Determine the Protein Corona with Possible Implications for Biological Impacts. *Proc. Natl. Acad. Sci. U.S.A.* **2008**, *105*, 14265–14270.
40. Rybak-Smith, M. J.; Tripisciano, C.; Borowiak-Palen, E.; Lamprecht, C.; Sim, R. B. Effect of Functionalization of Carbon Nanotubes with Psychosine on Complement Activation and Protein Adsorption. *J. Biomed. Nanotechnol.* **2011**, *7*, 830–839.
41. Tenzer, S.; Docter, D.; Rosfa, S.; Wlodarski, A.; Kuharev, J.; Rekik, A.; Knauer, S. K.; Bantz, C.; Nawroth, T.; Bier, C.; *et al.* Nanoparticle Size Is a Critical Physicochemical Determinant of the Human Blood Plasma Corona: A Comprehensive Quantitative Proteomic Analysis. *ACS Nano* **2011**, *5*, 7155–7167.
42. Kim, H. R.; Andrieux, K.; Delomenie, C.; Chacun, H.; Appel, M.; Desmaele, D.; Taran, F.; Georgin, D.; Couvreur, P.; Taverna, M. Analysis of Plasma Protein Adsorption onto PEGylated Nanoparticles by Complementary Methods: 2-DE, CE and Protein Lab-on-Chip System. *Electrophoresis* **2007**, *28*, 2252–2261.
43. Monopoli, M. P.; Walczyk, D.; Campbell, A.; Elia, G.; Lynch, I.; Bombelli, F. B.; Dawson, K. A. Physical−Chemical Aspects of Protein Corona: Relevance to *In Vitro* and *In Vivo* Biological Impacts of Nanoparticles. *J. Am. Chem. Soc.* **2011**, *133*, 2525–2534.
44. Ge, C.; Du, J.; Zhao, L.; Wang, L.; Liu, Y.; Li, D.; Yang, Y.; Zhou, R.; Zhao, Y.; Chai, Z.; *et al.* Binding of Blood Proteins to Carbon Nanotubes Reduces Cytotoxicity. *Proc. Natl. Acad. Sci. U.S.A.* **2011**, *108*, 16968–16973.
45. Moghimi, S. M.; Andersen, A. J.; Hashemi, S. H.; Lettiero, B.; Ahmadvand, D.; Hunter, A. C.; Andresen, T. L.; Hamad, I.; Szebeni, J. Complement Activation Cascade Triggered by PEG-PL Engineered Nanomedicines and Carbon Nanotubes: The Challenges Ahead. *J. Controlled Release* **2010**, *146*, 175–181.
46. Hamad, I.; Hunter, A. C.; Szebeni, J.; Moghimi, S. M. Poly-(ethylene glycol)s Generate Complement Activation Products in Human Serum through Increased Alternative Pathway Turnover and a MASP-2-Dependent Process. *Mol. Immunol.* **2008**, *46*, 225–232.
47. Deng, Z. J.; Liang, M.; Monteiro, M.; Toth, I.; Minchin, R. F. Nanoparticle-Induced Unfolding of Fibrinogen Promotes Mac-1 Receptor Activation and Inflammation. *Nat. Nanotechnol.* **2011**, *6*, 39–44.
48. Treuel, L.; Malissek, M.; Gebauer, J. S.; Zellner, R. The Influence of Surface Composition of Nanoparticles on Their Interactions with Serum Albumin. *ChemPhysChem* **2010**, *11*, 3093–3099.
49. Kasper, J.; Hermanns, I.; Bantz, C.; Maskos, M.; Stauber, R. H.; Pohl, C.; Unger, R.; Kirkpatrick, J. C. Inflammatory and Cytotoxic Responses of an Alveolar-Capillary Coculture Model to Silica Nanoparticles: Comparison with Conventional Monocultures. *Part. Fibre Toxicol.* **2011**, *8*, 1–16.
50. Scherer, C.; Noskov, S.; Utech, S.; Bantz, C.; Mueller, W.; Krohne, K.; Maskos, M. Characterization of Polymer Nanoparticles by Asymmetrical Flow Field Flow Fractionation (Af-Fff). *J. Nanosci. Nanotechnol.* **2010**, *10*, 6834–6839.